

High-resolution analysis of early diagenetic effects on magnetic minerals in post-middle-Holocene continental shelf sediments from the Korea Strait

Jian Liu,^{1,2} Rixiang Zhu,² Andrew P. Roberts,³ Shaoquan Li,¹ and Jeong-Hae Chang⁴

Received 25 September 2003; accepted 15 October 2003; published 10 March 2004.

[1] Two studied sediment cores from the Korea Strait contain mud sequences (14 m and 32.62 m in thickness) that were deposited during the last 6,000 years. The sediments have uniform lithology and geochemical properties, however, marked down-core changes in magnetic properties suggest that diagenesis has significantly impacted the magnetic properties. An expanded view of early diagenetic reactions that affect magnetic mineral assemblages is evident in these rapidly deposited continental shelf sediments compared to deep-sea sediments. The studied sediments are divided into four descending intervals, based on magnetic property variations. Interval 1 is least affected by diagenesis and has the highest concentrations of detrital magnetite and hematite, and the lowest solid-phase sulfur contents. Interval 2 is characterized by the presence of paramagnetic pyrite and sharply decreasing magnetite and hematite concentrations, which suggest active reductive dissolution of detrital magnetic minerals. Interval 3 is marked by a progressive loss of hematite with depth, and coincides with the minimum magnetite concentration. Interval 4 has an increasing down-core enhancement of authigenic greigite, which apparently formed at depths of 3–30 m below the sediment-water interface due to arrested pyritization reactions. These results indicate delays of thousands of years for acquisition of magnetizations carried by greigite, which suggests that studies of geomagnetic field behavior from greigite-bearing continental shelf sediments should be conducted with care. Also, virtually complete destruction of detrital magnetic minerals at depth suggests that magnetic studies of rapidly deposited shelf sediments are unlikely to provide a meaningful signature associated with syn-depositional environmental processes.

INDEX TERMS: 1512 Geomagnetism and Paleomagnetism: Environmental magnetism; 1519 Geomagnetism and Paleomagnetism: Magnetic mineralogy and petrology; 1540 Geomagnetism and Paleomagnetism: Rock and mineral magnetism; *KEYWORDS:* magnetite diagenesis, continental shelf sediments, rock magnetism, post-middle Holocene, Korea Strait

Citation: Liu, J., R. Zhu, A. P. Roberts, S. Li, and J.-H. Chang (2004), High-resolution analysis of early diagenetic effects on magnetic minerals in post-middle-Holocene continental shelf sediments from the Korea Strait, *J. Geophys. Res.*, 109, B03103, doi:10.1029/2003JB002813.

1. Introduction

[2] Post-depositional early diagenetic dissolution of detrital magnetite has been widely documented in marine sediments from relatively deep-water environments (generally with water depths more than 200 m), such as the

continental slope [Karlin, 1990a], deep-water shelf basins [Leslie *et al.*, 1990], or hemipelagic or abyssal plain settings [Karlin and Levi, 1983, 1985; Karlin, 1990b; Dekkers *et al.*, 1994; Vigliotti, 1997; Roberts *et al.*, 1999; Robinson *et al.*, 2000]. Bacterial metabolism of organic matter leads to consumption of oxygen in the sediment pore waters. Subsequent suboxic and anoxic conditions give rise to diagenetic reactions that involve the reductive dissolution of detrital magnetite and other iron-bearing phases as well as to the (bio)authigenic formation of new magnetic minerals [Stolz *et al.*, 1986; Canfield and Berner, 1987; Karlin *et al.*, 1987; Roberts and Turner, 1993; Sakaguchi *et al.*, 1993; Tarduno, 1994; Larrasoana *et al.*, 2003]. Understanding the impact of early diagenesis on magnetic minerals has been important for interpreting sedimentary paleomagnetic and environmental magnetic records [e.g., Snowball and Thompson, 1990; Verosub and Roberts, 1995; Stockhausen

¹Qingdao Institute of Marine Geology, China Geological Survey, Qingdao, China.

²Institute of Geology and Geophysics, Chinese Academy of Sciences, Beijing, China.

³School of Ocean and Earth Science, University of Southampton, Southampton Oceanography Centre, Southampton, UK.

⁴Korean Institute of Geology, Mining and Material, Taejeon, Korea.

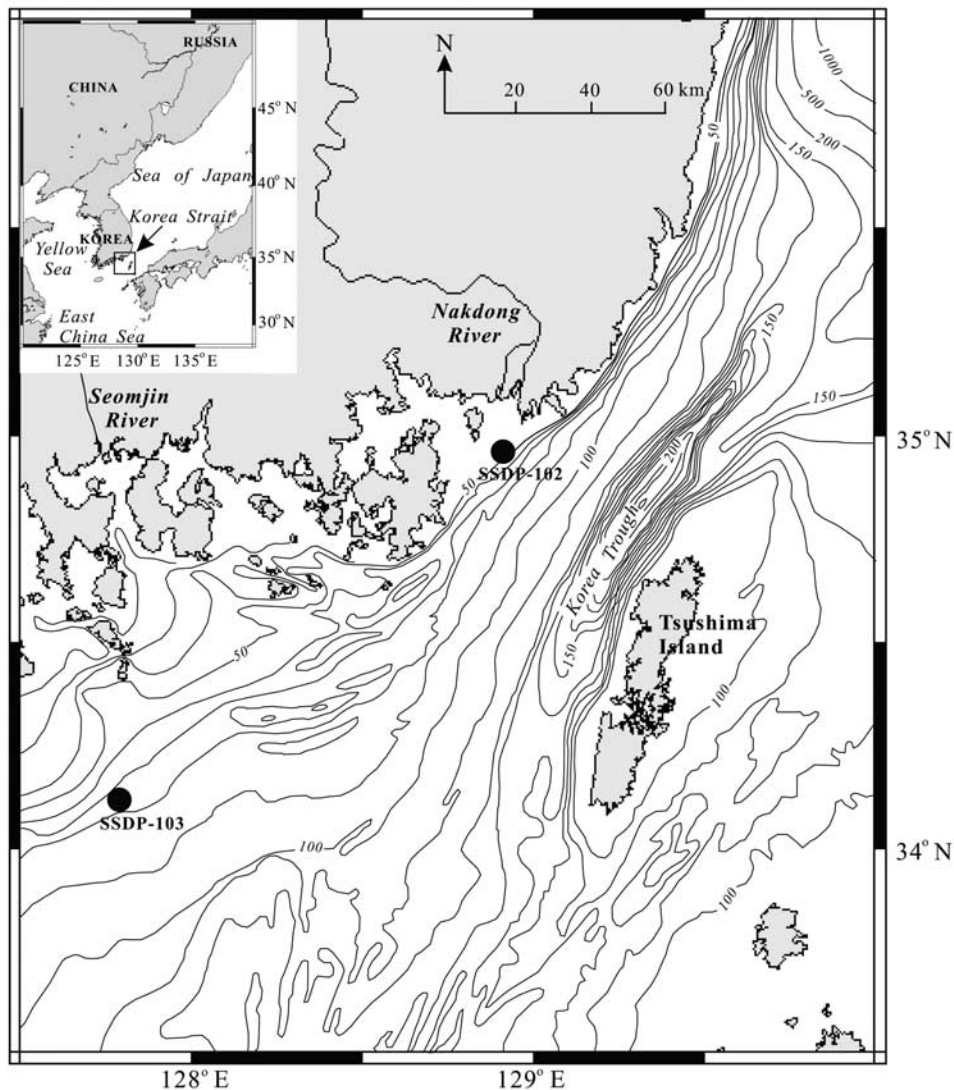


Figure 1. Map of the Korea Strait with bathymetry and location of the SSDP-102 and SSDP-103 cores (modified after Yoo *et al.* [2003]). Water depths are in meters.

and Thouveny, 1999]. Despite progress made through the study of deep-sea sediments, some diagenetic processes, such as the detailed behavior of detrital hematite and the environmental controls on the abundance, distribution and preservation of (bio)authigenic magnetic minerals, are not well understood.

[3] Detailed studies of the effects of early diagenesis on magnetic minerals in shallow continental shelf sediments (less than 100 m water depths), where young, rapidly deposited sediments are expected to be actively undergoing suboxic organic matter diagenesis, are sparse. Studies from deeper water settings involve sediments deposited at slower rates than on the continental shelf. We present results of a magnetic and geochemical investigation of muddy continental shelf sediments from the Korea Strait (Figure 1), which were extremely rapidly deposited over the last ~6,000 years (~2.3–5.1 m/kyr). The objective of this work was to obtain high-resolution magnetic records of early diagenetic processes in the rapidly deposited shelf sequence in an attempt to clarify processes that have not

been completely unraveled in previous studies of deep-sea sediments.

2. Geological Setting and Stratigraphy

[4] The Korea Strait is located between the southeastern tip of the Korean Peninsula and Tsushima Island (Figure 1). It is a narrow continental shelf (about 60 km wide) that connects the East China Sea and the Sea of Japan. Morphologically, the shelf can be divided into three distinct regions: inner shelf (<80 m water depth), mid-shelf (80–120 m depth), and outer shelf (>120 m depth) [Yoo and Park, 1997]. The inner shelf is flat and smooth, and is covered by recent muddy deposits derived from the Nakdong and Seomjin Rivers [Park and Yoo, 1988]. The mid-shelf is largely covered with sandy sediments containing large amounts of gravel and shell debris and is partly occupied by a series of sand ridges, which were formed during the Holocene sea level transgression [Park and Yoo, 1992; Yoo and Park,

2000]. The outer shelf contains a trough, which is an elongated structural depression that reaches depths of 230 m, in which gravelly muddy sand and sandy mud is being deposited.

[5] The Korea Strait is a seaway that is dominated by the northeastward-flowing Tsushima Current, which is a branch of the Kuroshio Warm Current. The current speed ranges between about 0.3 and 0.9 m/s; it is strongest in the summer and weakest in the winter [Yoo and Park, 1997]. The near-coastal area is dominated by tidal currents that generally flow northeastward during ebb and southwestward during flood, with a maximum velocity of 0.9 m/s [Ro et al., 1995]. A coastal current is also reported to flow northeastward along the southeastern coast of the Korean Peninsula [Kim et al., 1986]. The Nakdong and Seomjin Rivers are two major inland fluvial systems that deliver voluminous amounts of sediment and freshwater to the Korea Strait shelf, discharging into the Korea Strait about 1.0×10^7 tons and 0.8×10^6 tons of sediment per year, respectively [Park et al., 1996]. The sediments from both rivers are completely confined to the inner shelf and are mostly transported northeastward by strong shelf currents.

[6] A great deal of work has been done to unravel the evolution of late Quaternary deposits in the Korea Strait [e.g., Park and Yoo, 1988, 1992; Park et al., 1990, 1995, 1996, 2000; Park and Lee, 1994; Yoo et al., 1996; Korean Institute of Geology, Mining and Materials, 2000], and characteristic sedimentation patterns that occurred in response to late-Quaternary cyclic fluctuations in relative sea level have been revealed. On the basis of high-resolution seismic profiles, Yoo and Park [1997] identified a distinct pattern of stacked progradational sedimentary wedges on the shelf margin and trough region, which comprise a succession of three distinct units (A = lower, B = middle, C = upper) that are bounded by erosional unconformities. These wedges thicken seaward and their landward limit lies at about 90–120 m water depth. They are interpreted to have been formed during late Quaternary glacioeustatic sea level lowstands when multiple falls of sea level were coupled with high sediment discharge from the paleo-Nakdong River system. The youngest wedge (upper unit C) is interpreted to have been deposited during the last glacial period, based on ^{14}C convention dating [Yoo and Park, 1997]. The mid-shelf sandy sediments, which cover some landward parts of the above mentioned wedges, contain abundant shell fragments and gravels and were interpreted to have formed close to the shoreline [Park and Yoo, 1992], and were reworked and shaped during the Holocene transgression from 15,000 to 6,000 years BP [Yoo and Park, 2000]. On the basis of the newest AMS ^{14}C convention datings, Park et al. [2003] suggested that the mid-shelf sand ridges developed in the middle-Holocene transgression (corresponding to about 9,500 to 5,500 years BP). The inner-shelf muddy deposits, which drape the landward parts of the middle-shelf sandy sediments, thin seaward from thicknesses of more than 40 m in onshore areas until they disappear at water depths of about 80–100 m [Park et al., 1999]. The fact that the inner shelf muddy deposits drape the middle Holocene transgressive sands

demonstrates that they were deposited during the last $\sim 6,000$ years when Holocene sea levels were highest. The outer-shelf sedimentary wedge (low-stand systems tract), the middle-shelf sandy deposits (transgressive systems tract) and the inner-shelf muddy sediments (highstand systems tract) [e.g., Yoo and Park, 2000] are clearly visible in high-resolution seismic profiles and the boundaries between these systems tracts are interpreted to have resulted from sea level changes during the past $\sim 20,000$ years [e.g., Yoo and Park, 1997; Park et al., 2000, 2003]. In summary, many previous studies have demonstrated that the inner-shelf muddy sediments were deposited during the post middle-Holocene, after the post-glacial transgression peaked. The sediment distribution pattern in the Korea Strait suggests that most fine-grained sediment derived from the two major rivers is trapped on the inner shelf [Park et al., 1996; Yoo and Park, 2000] and that these sediments settled out of suspension rather than being deposited as a result of large sediment discharge events.

[7] Two cores, SSDP-102 and SSDP-103, were recovered from the Korea Strait in 1998 and 1999, respectively, by the Korean Institute of Geology, Mining and Material (KIGMAM) (Figure 1). Core SSDP-102 (31.6 m in length) was acquired to the south of the Nakdong River mouth ($34^{\circ}57.2'N$, $128^{\circ}52.9'E$) at a water depth of about 40 m, while core SSDP-103 (72.4 m in length) was retrieved southwest of core SSDP-102 at a water depth of about 72 m, about 100 km south of the Seomjin River mouth ($34^{\circ}7.191'N$, $127^{\circ}40.871'E$). The uppermost 14 m and 30.62 m of the SSDP-102 and SSDP-103 cores, respectively, are dominated by homogeneous mud (clayey silt) (Figures 2a and 3a). Core recovery rates for the mud were better than 90%. The mud sections in both cores were interpreted, based on high-resolution seismic reflection profiles and lithological characteristics, as the highstand systems tract that formed after post-glacial sea level rise peaked at about 6,000 years B.P. [Yoo et al., 2003]. Calibrated AMS ^{14}C dates from Core SSDP-102 [Nam et al., 2003] suggest that the mud section formed after 5.1 cal ka BP, which is in good agreement with previous coring and sequence stratigraphic interpretations for these shelf sediments. On the basis of the thickness of the highstand systems tract and the time interval over which it was deposited, Park et al. [1996] estimated sedimentation rates of 1–4 m/kyr for the mud unit. This longer-term estimate is consistent with ^{210}Pb dates from the youngest sediments recovered in cores from the inner shelf (1.8–4.4 mm/year) and is consistent with the present rate of discharge of suspended riverine sediments into the area [Park et al., 1996, 1999]. If it is assumed that the highstand systems tract was deposited at uniform rates between 6,000 years B.P. and the present, the Holocene muds in cores SSDP-102 and SSDP-103 (14 m and 30.62 m in thickness, respectively) would have been deposited at average rates of ~ 2.3 –5.1 m/kyr, which is the same order of magnitude provided by the estimates described above. The inferred high sedimentation rates of these muddy sediments are comparable to those of post-glacial muddy deposits in the southeastern Yellow Sea [Jin and Chough, 1998] and the Holocene mud wedge

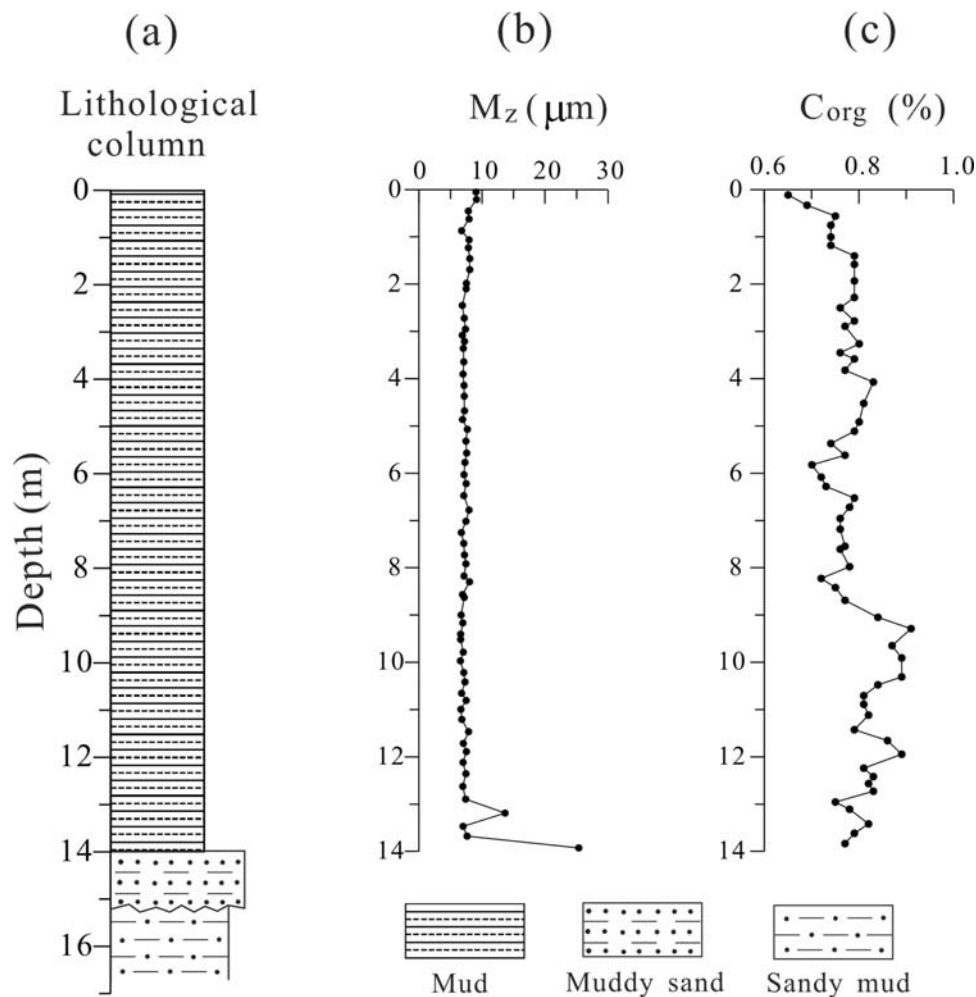


Figure 2. (a) Lithological log for the uppermost 16 m of the SSDP-102 core, with (b) down-core variations of the average grain size (M_z), and (c) organic carbon content (C_{org}). The upper mud section (0 to 14 m), which represents the modern marine environment, was formed after 5.1 cal ka BP [Nam *et al.*, 2003; Yoo *et al.*, 2003]. The muddy-sand section between 14 and 15.1 m, which represents transgressive lag deposits produced through shoreface erosion during the post-glacial transgression, was formed between 6.2 and 5.1 cal ka BP [Nam *et al.*, 2003; Yoo *et al.*, 2003] (see text for discussion).

in the area around the Shandong Peninsula, in the western Yellow Sea [Liu *et al.*, 2002].

3. Methods

[8] Cores SSDP-102 and SSDP-103 were sampled at KIGMAM for magnetic and geochemical analyses, with 8 cm³ plastic cubes taken at 5–7 cm and 8–12 cm intervals down the cores, respectively. The uppermost 14 m of the SSDP-102 core (240 samples) and the uppermost 30.62 m of the SSDP-103 core (207 samples) were sampled. The samples were brought to the Paleomagnetic Laboratory at the Institute of Geology and Geophysics, Chinese Academy of Sciences, Beijing, China, for magnetic measurements. All magnetic measurements were made using untreated, wet sediment samples, except for measurements of temperature-dependence of magnetic susceptibility, hysteresis loops and thermal demagnetization.

[9] Measurements of the natural remanent magnetization (NRM), low-frequency volume-specific magnetic susceptibility (χ), anhysteretic remanent magnetization (ARM), and isothermal remanent magnetization (IRM) were conducted in successive order. NRMs were measured on a 2-G Enterprises model 755R cryogenic magnetometer. χ was measured with a Bartington Instruments M.S. 2 magnetic susceptibility meter. ARMs were imparted with a Schonstedt GSD-1 alternating field (AF) demagnetizer, with a peak AF of 90 mT and a superimposed direct bias field of 0.05 mT. ARM and IRM measurements were performed with a JR-5A spinner magnetometer. IRMs were induced along one axis of the samples with a 2-G Enterprises model 660 pulse magnetizer in a 1.6 T pulsed field. We refer to this IRM as a saturation IRM (SIRM). A back-field IRM was then applied in the opposite direction with a 300 mT field ($\text{IRM}_{-300 \text{ mT}}$), and values of S_{300} ($= -\text{IRM}_{-300 \text{ mT}}/\text{SIRM}$) were calculated [King and Channell, 1991]. This parameter reflects the relative proportion of low coercivity to high coercivity

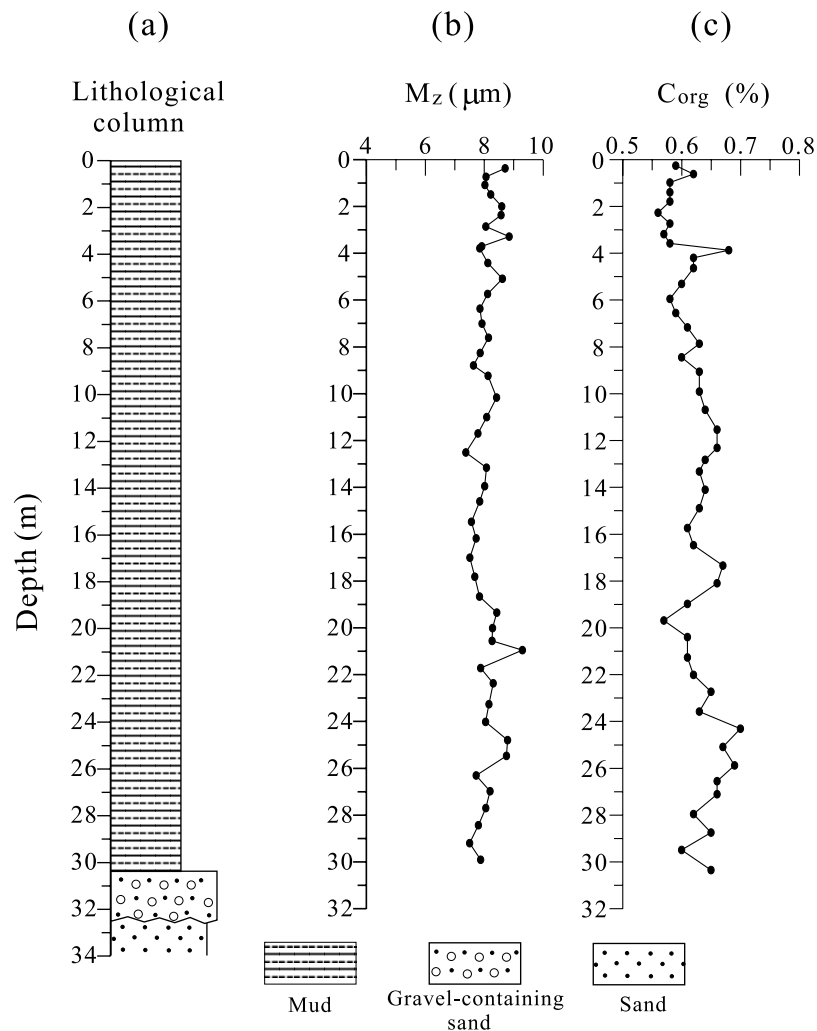


Figure 3. (a) Lithological log for the uppermost 34 m of the SSDP-103 core, with (b) down-core variations of the average grain size (M_z), and (c) organic carbon content (C_{org}).

magnetic minerals in a sample. To quantify the absolute concentration of high coercivity components, the HIRM ($= (\text{SIRM} + \text{IRM}_{-300 \text{ mT}})/2$) parameter [Thompson and Oldfield, 1986; Robinson, 1986] was evaluated. After the above mentioned magnetic parameters were measured, the samples were oven-dried at 40°C overnight and were weighed to enable calculation of mass-specific magnetic susceptibility (χ) and mass-specific values of ARM and SIRM.

[10] Some of the remaining sub-samples were used to carry out 3-axis thermal demagnetization experiments on a composite IRM [Lowrie, 1990] by applying fields of 2.7 T, 0.5 T and 0.05 T, respectively, along the 3 mutually perpendicular sample axes using a 2-G Enterprises model 660 pulse magnetizer, followed by thermal demagnetization at steps of $20\text{--}50^\circ$ from 80° to 700°C , using a MMTD60 thermal demagnetizer. These experiments were conducted in order to measure the demagnetization behavior of various coercivity fractions in the samples. The remanence measurements were made using a 2-G Enterprises model 755R cryogenic magnetometer.

[11] In addition to the above magnetic experiments, which were conducted for samples from both cores, the following measurements were made for samples from the

SSDP-102 core only: 1) magnetic hysteresis loops were measured for 56 representative, dried samples using an alternating gradient magnetometer (MicroMag 2900) in a maximum field of 1.5 T; 2) the temperature-dependence of magnetic susceptibility was measured in an argon atmosphere for representative samples ($\chi(T)$ curves) using a KLY 3s Kappabridge magnetic susceptibility meter with CS-3 high-temperature device; and 3) a Rigaku D/max-rA X-ray diffractometer was used to analyze the mineral composition of heavy-mineral concentrates in order to determine whether the samples contain pyrite.

[12] The organic carbon (C_{org}) content of sub-samples from the two cores was analyzed using a Leco CS-34 Carbon/Sulfur Determinator, with data precision better than 0.01%. These measurements were made at the Wuxi Institute of Experimental Geology, Research Institute of Petroleum Exploration and Production, SINOPEC. Fifty-seven samples were analyzed from the uppermost 14 m of the SSDP-102 core and 47 samples were analyzed from the uppermost 30.62 m of the SSDP-103 core. Samples were selected at stratigraphic intervals of 0.2–0.8 m for these analyses.

[13] Chemical element analyses of solid phases for samples from the post-middle-Holocene mud of both cores were made with a Phillips PW2404 X-ray fluorescence (XRF)

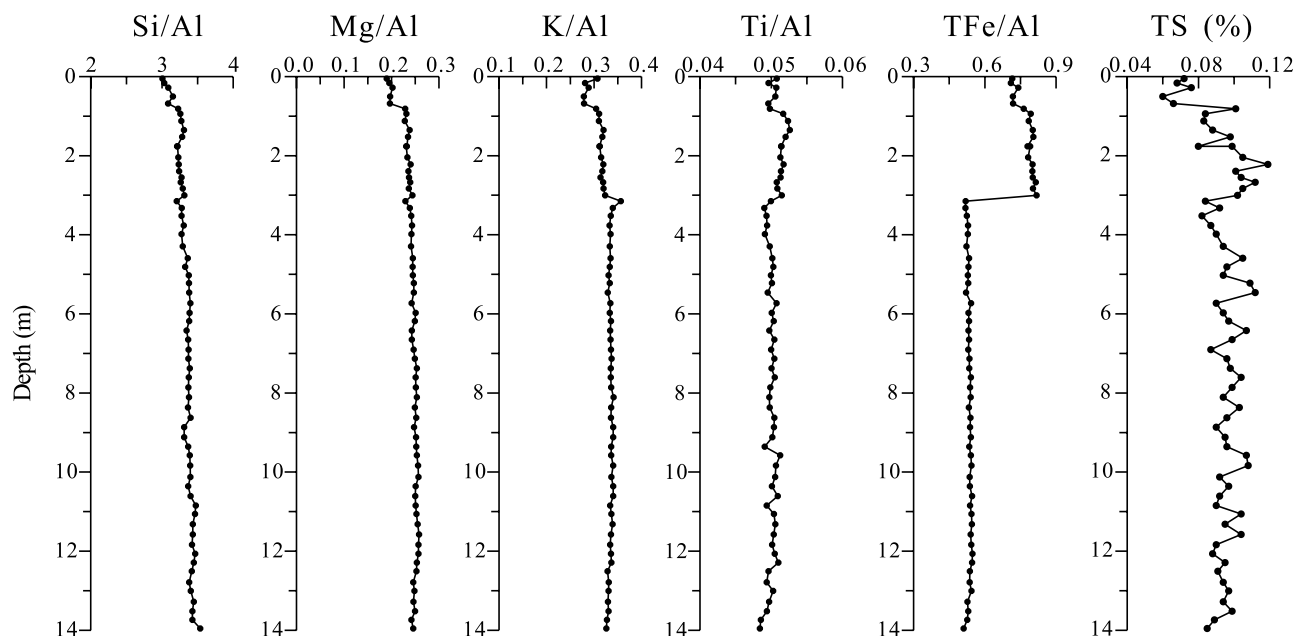


Figure 4. Chemical profiles of selected elements from the mud section of the SSDP-102 core. TFe = total Fe content; TS = total sulfur content.

spectrometer at the Beijing Research Institute of Uranium Geology. The samples were prepared by disaggregation in a ball mill; the data precision is better than 1%. Sixty-five samples were analyzed from the SSDP-102 core and 47 samples were analyzed from the SSDP-103 core, with samples taken at stratigraphic intervals of 0.2 to 0.8 m. Measurements of stratigraphic variations of total sulfur are available for the SSDP-102 core only. Additionally, 63 samples from the SSDP-102 core and 47 samples from the SSDP-103 core were taken at 0.2–0.8 m intervals to determine sediment grain sizes using a Mastersizer-2000 laser particle size analyzer in the Experiment-Testing Center of Marine Geology, Qingdao Institute of Marine Geology. Prior to grain-size analysis, the samples were pretreated with 6% H_2O_2 and 0.8% HCl to remove organic material and carbonate. The average grain sizes (M_z) of samples were calculated by the equation from *Folk and Ward* [1957].

4. Results

4.1. Lithology and Solid-Phase Geochemistry

[14] The lithological homogeneity of the mud sections in the two cores is evident in their grain-size distributions. Except two peaks below 13 m, small fluctuations in average grain size are observed for the mud section of the SSDP-102 core, with variations mostly between 6.5 and 8 μm (Figure 2b). In the SSDP-103 core, variation of the average grain size of the mud section is even smaller than for the SSDP-102 core, with changes largely between 7.5 and 8.8 μm (Figure 3b).

[15] The C_{org} content varies between 0.65 and 0.91% in the mud section of the SSDP-102 core (Figure 2c). It is less than 0.83% in the uppermost 9 m of the core and a little higher (between 0.75 and 0.91%) in the interval from 9 to 14 m. The mud section in the SSDP-103 core has slightly lower C_{org} contents (between 0.56 and 0.7%) compared to the corresponding part of the SSDP-102

core, with lowest values (mostly less than 0.6%) in the uppermost 4 m (Figure 3c).

[16] Profiles of selected elements from the mud section in both cores, including the major terrigenous elements (Si, Mg, K, and Ti) and those related to the diagenetic variation of magnetic minerals (total Fe and S), are shown in Figures 4 and 5. In the uppermost 14 m of the SSDP-102 core (Figure 4), Si, Mg and K contents increase slightly down-core from the surface to about 5 m and then remain relatively constant. Ti and total Fe exhibit higher abundances in the upper 3 m than in the underlying part of the core. Sulfur values increase from 0.06–0.076% in the uppermost 0.78 m and then to 0.08–0.119% in the mud below 0.78 m, presumably due to pore water sulfate reduction and the formation of iron sulfide minerals [Karlin, 1990a].

[17] In the mud section of the SSDP-103 core, Si, Mg and K variations are relatively invariable with no discernable trends (Figure 5). Overall Ti contents and total Fe contents do not undergo large variations, which suggests that the marked magnetic property variations are largely due to the diagenetically induced mineral phase changes.

[18] In summary, the sediment grain size and chemistry of the mud sections suggest that the lithology is uniform and that no major source-related grain size or chemical changes have occurred in the studied sediments. This is consistent with the relatively stable marine conditions on the continental shelf with only small-scale sea level fluctuations (several meters) since the post-middle-Holocene [Zhao, 1984; Saito, 1993]. Moreover, the mud below 0.78 m in the SSDP-102 core appears to have been subject to sulfate reduction, as evidenced by increased sulfur accumulations below this depth (Figure 4).

4.2. Down-Core Variations in Magnetic Parameters

[19] For the mud section in the SSDP-102 core, five concentration-dependent magnetic parameters (NRM, χ , ARM, SIRM and HIRM), and the magnetic mineralogy-

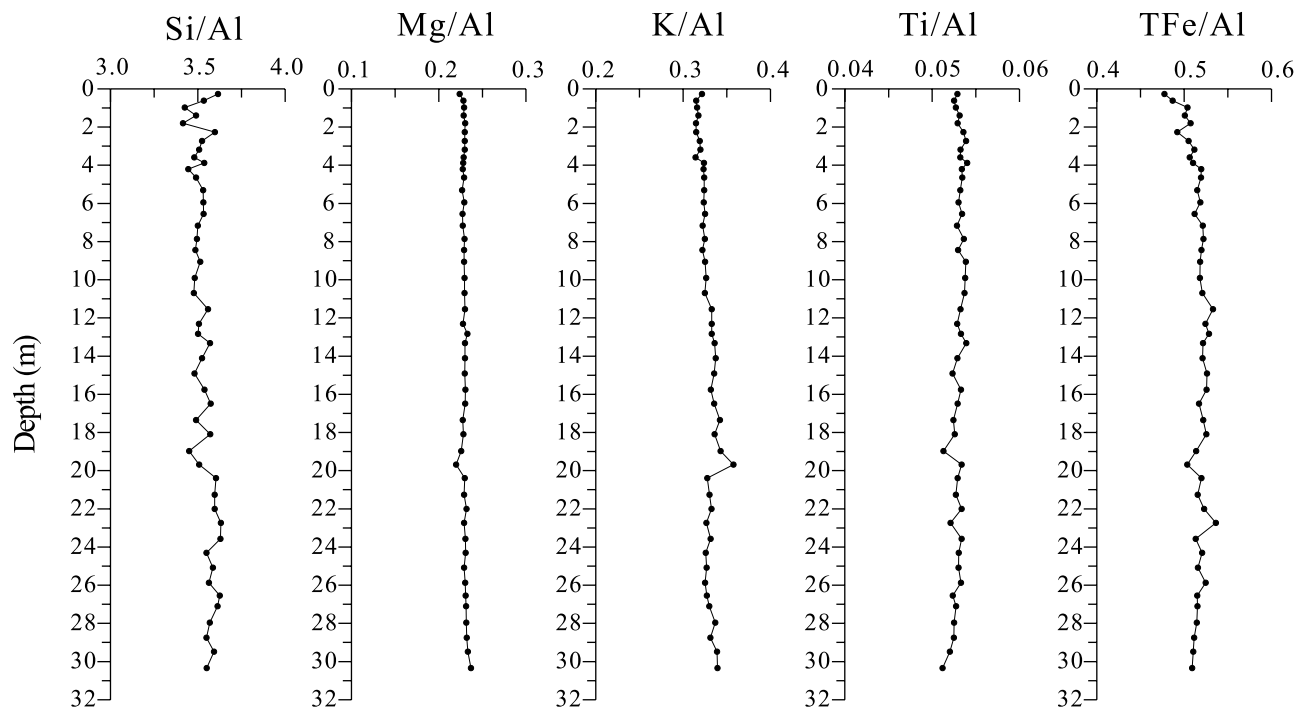


Figure 5. Chemical profiles of selected elements from the mud section of the SSDP-103 core. TFe = total Fe content.

related parameter (S_{300}) have relatively high values in the uppermost 0.78 m. These values undergo a precipitous down-core drop from 0.78 to 1.90 m (Figure 6), which is diagnostic of early diagenesis in deep-water marine sedimentary sequences [Karlin and Levi, 1985; Robinson et al., 2000]. The diagenetic chemical reactions reflect a decrease in the magnetic mineral content resulting from preferential dissolution of fine-grained ferrimagnetic minerals and diagenetic formation of pyrite. The presence of pyrite in the mud section of the SSDP-102 core below 0.78 m (and below 0.49 m in core SSDP-103) was confirmed by XRD analysis of heavy-mineral concentrates from representative samples. This indicates that sulfate-reducing conditions were reached in the sediments during early diagenesis [Canfield and Berner, 1987]. We can divide the entire mud section in the uppermost 14 m of core SSDP-102 into 4 intervals, in descending order, according to variations of these six magnetic parameters.

[20] Interval 1 (0 to 0.78 m): the 6 parameters have the highest values for the entire mud section in this interval. S_{300} values suggest that this interval is magnetically dominated by low coercivity ferrimagnetic minerals.

[21] Interval 2 (0.78 to 1.90 m): with the exception of HIRM, the concentration-dependent magnetic parameters decline rapidly with depth in the upper 30 cm of this interval, and then decrease slightly down-core except for NRM and ARM which have consistently low values after the marked decline. S_{300} values drop sharply from 0.85 at the top of this unit to around 0.6 at about 1.08 m, followed by a slight overall decrease with depth with the lowest value, 0.51, occurring at 1.90 m. These changes indicate that the dominant magnetic minerals rapidly change down-core from low coercivity ferrimagnetic components to high

coercivity minerals. HIRM values progressively decrease down-core in the upper part of this interval, and then remain roughly stable in the lower part, indicating that the partial depletion of high coercivity minerals took place mostly in the upper mud of this unit.

[22] Interval 3 (1.90 to 3.24 m): SIRM continues to slowly decrease down-core, reaching the lowest value in the entire mud section at the bottom of this unit. χ decreases slightly down-core and also reaches its lowest values at the base of this interval. ARM and NRM values remain constantly low as in the lower part of Interval 2. HIRM undergoes a nearly monotonic decrease down to the base of this interval. In contrast to the other 5 parameters, S_{300} increases rapidly downward from a value of 0.51 at 1.90 m to a value of 0.80 at 3.24 m. The clear inverse relationship with HIRM suggests that the down-core increase in S_{300} values is completely due to the rapid preferential depletion of high coercivity minerals with depth. The 5 concentration-dependent magnetic parameters all decrease greatly from Interval 1 to the base of Interval 3. Compared to mean values in Interval 1, χ values fall by 71%, SIRM by 93%, ARM by 97%, and HIRM by 88%. The differences between the percentage losses for these parameters can be attributed to their respective sensitivities to the presence of fine-grained ferrimagnetic minerals.

[23] Interval 4 (3.24 to 14 m): although this interval has low values for the 5 concentration-dependent magnetic parameters, when plotted on a logarithmic scale on a carbonate-free basis, variations of these parameters are more clearly evident (Figure 6b) and are observed to be different for the various parameters. NRM and SIRM undergo a gradual increase down-core. χ is nearly constant with depth. ARM fluctuates markedly with no systematic changes.

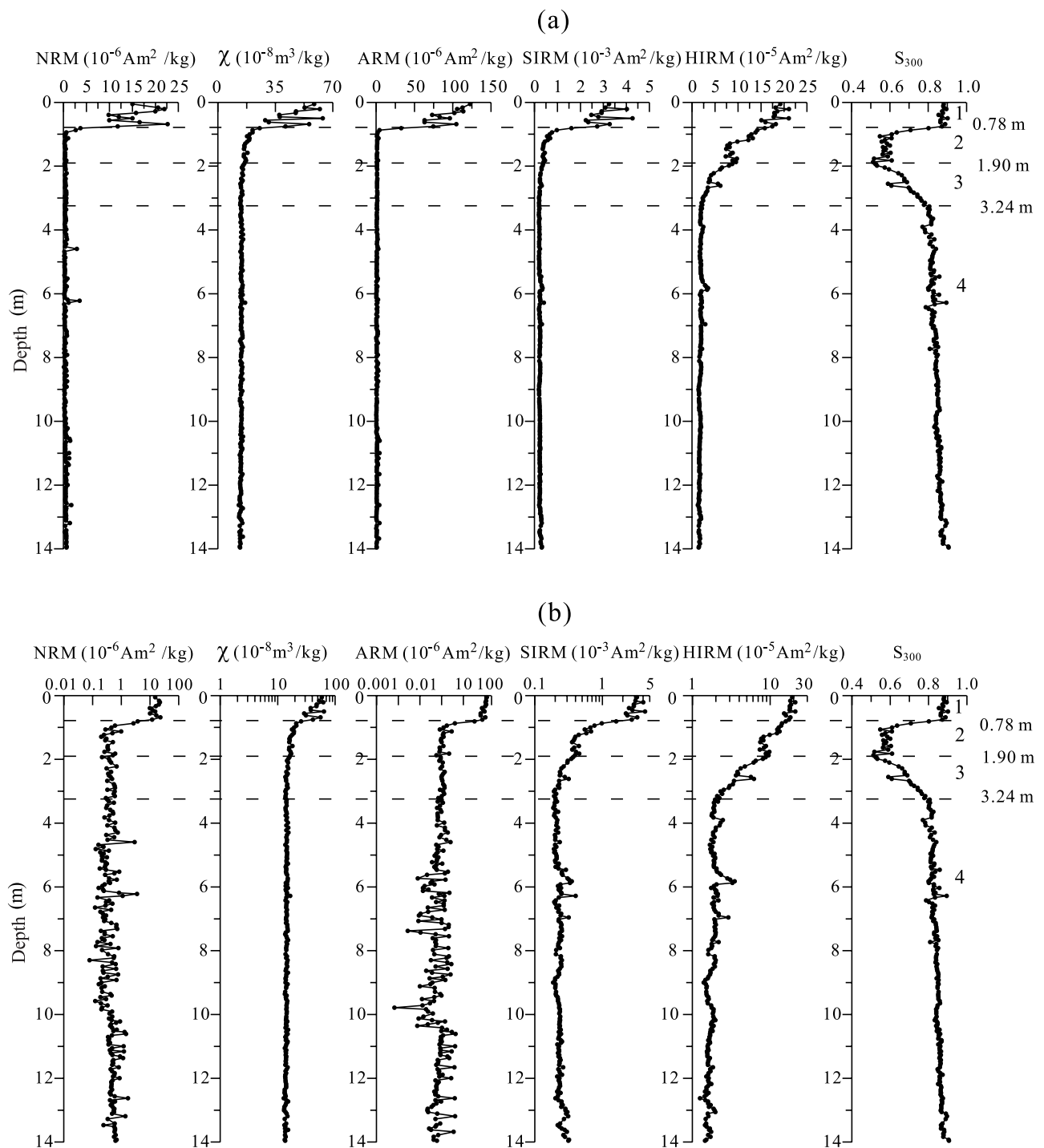


Figure 6. Down-core variations of concentration-dependent magnetic parameters, including: NRM, χ , ARM, SIRM and HIRM, and the magnetic mineralogy-related parameter S_{300} for the mud section of the SSDP-102 core. The dashed horizontal lines indicate the boundaries of different magnetic intervals, which are the same as in Figure 10a. (a) All magnetic parameters are expressed on a bulk-sediment basis and are plotted on linear scales. (b) The 5 concentration-dependent magnetic parameters are expressed on a carbonate-free basis and are plotted on logarithmic scales, while S_{300} is plotted on a linear scale. The mud section can be distinctively divided into four intervals based on variations of magnetic parameters. Interval 1: 0 to 0.78 m; Interval 2: 0.78 to 1.90 m; Interval 3: 1.90 to 3.24 m; and Interval 4: 3.24 to 14 m.

IRM undergoes some gradual, but minor, variations. Following the increasing trend observed in the overlying interval, S_{300} slowly increases from 3.24 m down to 14 m, with values rising from about 0.8 at the top to 0.91 at the base, which reflects an increasing contribution from low coercivity ferrimagnetic minerals with depth.

[24] The 6 parameters in the mud section of the SSDP-103 core undergo similar patterns of variation to those observed in the uppermost 14 m of the SSDP-102 core. The mud section of the SSDP-103 core can therefore also be subdivided into the same 4 intervals (Figure 7) in terms of variations of the 6 measured parameters, although the intervals defined in both cores have different thicknesses presumably due to different sedimentary and diagenetic conditions at the two sites depending on sedimentation rate, organic carbon content, etc.

4.3. Magnetic Mineralogy

[25] Representative $\chi(T)$ curves for heating-cooling cycles from room temperature up to 700°C for the different intervals noted above in the mud section of the SSDP-102 core are shown in Figure 8. For samples from Interval 1 (Figure 8a), χ slowly increases until about 520°C, and then decreases sharply to near zero at ~580°C, which suggests that magnetite is the dominant magnetic mineral. Upon cooling, a marked increase in χ occurs between 580 and 400°C, which indicates the production of a significant amount of magnetite during heating.

[26] For samples from Interval 2 and Interval 3 (Figure 8b), χ decreases slowly from room temperature to ~300°C, which suggests a dominant contribution from paramagnetic minerals. This probably reflects the increased relative contribution of paramagnetic clays to the susceptibility as a result of diagenetic destruction of magnetite and the formation of pyrite in its place. The decrease in χ up to ~300°C is followed by an increase in χ from 300 to 440°C, which could have been caused partially by the thermally induced conversion of iron-bearing silicate or clay minerals into magnetite and partially by the conversion of diagenetically formed paramagnetic pyrite into magnetite within this temperature range [e.g., Roberts and Pillans, 1993]. The presence of newly formed magnetite is indicated by the gradual decrease in χ from 460° up to 580°C. During cooling, the $\chi(T)$ curves are similar to those from Interval 1.

[27] For samples from Interval 4 (Figure 8c), $\chi(T)$ curves in the heating-cooling cycle are similar to those of samples from Interval 2, except for a marked increase in χ from ~300° to about 500°C. The sharp increase in χ at ~300°C could be due to the presence of greigite, and might signal the onset of thermal alteration of greigite into magnetite or maghemite [Geiss and Banerjee, 1997; Dekkers et al., 2000].

[28] Typical thermal demagnetization curves of a composite 3-axis IRM [Lowrie, 1990] for samples from different intervals in both cores are shown in Figure 9. For samples from Interval 1, most of the IRM resides in the low coercivity (<0.05 T) and medium coercivity (0.05 to 0.5 T) fractions (Figure 9a). The low coercivity fraction undergoes gradual decay up to 550°C and a sharp unblocking at around 580°C (Figure 9a), with the former probably reflecting gradual unblocking resulting from the presence of a grain size distribution and the latter indicating magnetite

as a major carrier of remanent magnetization. The medium coercivity fraction (0.05 to 0.5 T) undergoes two marked unblocking events at about 580°C and 680°C, which are characteristic of magnetite and hematite, respectively. The high coercivity fraction (0.5 to 2.7 T) undergoes a smoothly monotonic decay until its unblocking at about 680°C, which is indicative of hematite. Samples from Intervals 2 and 3 yield somewhat similar results to those from Interval 1, except that the low coercivity fraction represents a much smaller portion of the total IRM (Figures 9a and 9b), which is consistent with the greater relative proportion of high coercivity minerals present (as indicated by lower values of S_{300} in these two intervals compared to Interval 1).

[29] The most distinct difference for samples from Interval 4, compared to those from higher parts of the core, is that the high coercivity fraction undergoes a considerable decrease from 200° to 320°C (Figures 9c and 9d). Greigite has higher coercivities than magnetite [Roberts, 1995] and is characterized by loss of most of its magnetization from 200° to 350°C [Snowball, 1991; Krs et al., 1992; Reynolds et al., 1994; Roberts, 1995; Torii et al., 1996]. We therefore attribute the rapid decay of magnetization in the high coercivity fraction within the 200–320°C temperature window to the presence of greigite, which is also suggested by a sharp increase in the magnetic susceptibility at around 300°C. In contrast, pyrrhotite undergoes rapid unblocking within a much narrower temperature range of 320–350°C [Dekkers, 1989; Torii et al., 1996]. The behavior of the high coercivity fraction rules out the possibility that the loss in magnetization at around 200–320°C is due to maghemite or titanomagnetite because the low and medium coercivity fractions do not undergo similar prominent decays in the 200–320°C temperature window as the high coercivity component. We interpret this difference to the likelihood that the thermal demagnetization of greigite in the two lower coercivity fractions is obscured by the gradual unblocking of maghemite and/or titanomagnetite. Finally, all three coercivity fractions unblock to near-zero values at about 580°C, which suggests that magnetite is also present and that there is little hematite in Interval 4.

[30] On the basis of the $\chi(T)$ curves and thermal demagnetization of a composite 3-axis IRM, we conclude that magnetite is the dominant magnetic mineral in Interval 1, and that the magnetic properties of intervals 2 and 3 from both cores contain substantial contributions from hematite as well as magnetite. In contrast, the magnetic mineralogy of Interval 4 is characterized by magnetite and greigite, with little hematite.

4.4. Magnetic Granulometry

[31] After removal of the paramagnetic slope at high fields, which is considered to be related largely to the clay matrix in the samples, the saturation magnetization (M_s), the saturation remanent magnetization (M_{rs}), the coercive force (H_c) and the coercivity of remanence (H_{cr}) were determined for 56 samples from the mud section of the SSDP-102 core. Down-core profiles of M_{rs}/M_s and H_{cr}/H_c are shown in Figure 10a. Marked differences are evident for the four intervals. However, the magnetic mineralogy is only dominated by a ferrimagnetic phase in Interval 1 and Interval 4, as suggested by the higher values of S_{300} (Figure 6), so we only plot the hysteresis parameters (M_{rs}/M_s and H_{cr}/H_c) on a

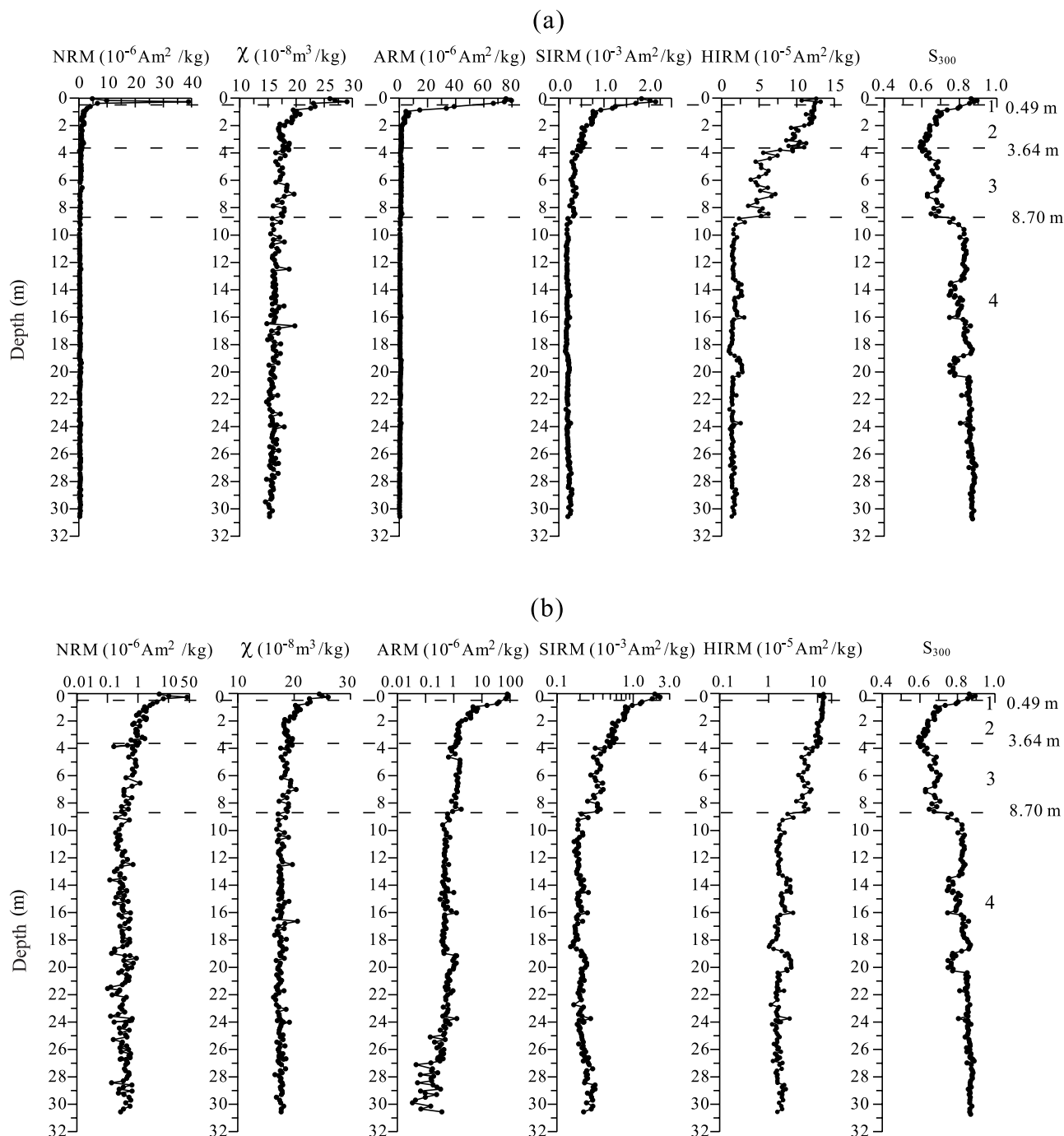


Figure 7. Down-core variations of concentration-dependent magnetic parameters, including: NRM, χ , ARM, SIRM and HIRM, and the magnetic mineralogy-related parameter S_{300} for the mud section of the SSDP-103 core. (a) All magnetic parameters are expressed on a bulk-sediment basis and plotted on linear scales. (b) The 5 concentration-dependent magnetic parameters are expressed on a carbonate-free basis and are plotted on logarithmic scales, while S_{300} is plotted on a linear scale. The mud section can also be divided into four intervals as is the case in the SSDP-102 core. Interval 1: 0 to 0.49 m; Interval 2: 0.49 to 3.64 m; Interval 3: 3.64 to 8.70 m; and Interval 4: 8.70 to 30.62 m.

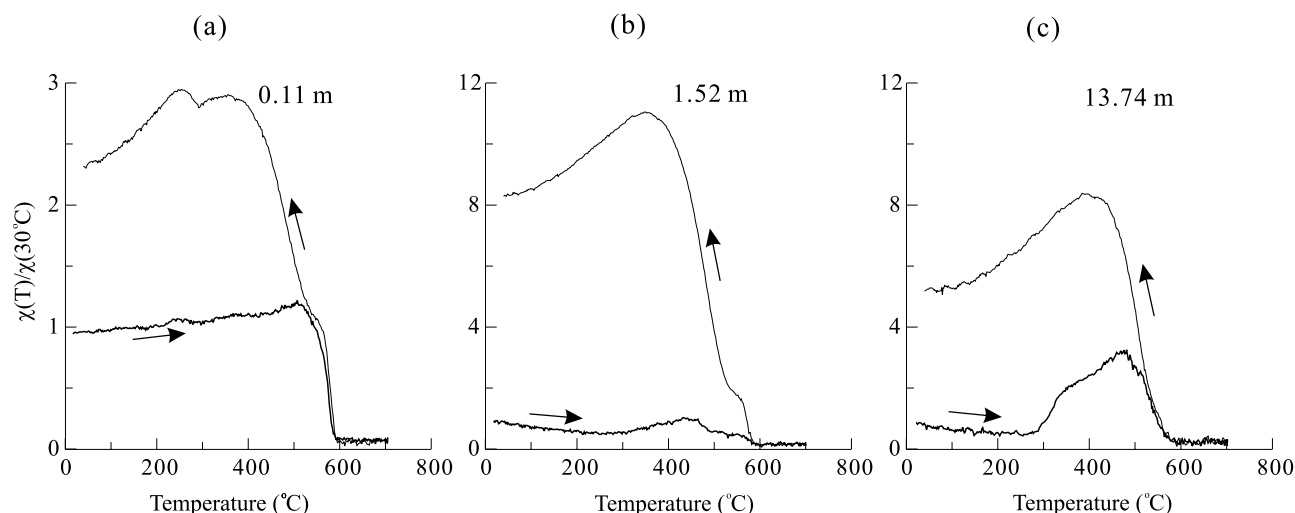


Figure 8. Typical temperature dependence of magnetic susceptibility curves (heating and cooling cycles) for different intervals of the SSDP-102 core. (a) Interval 1, (b) Intervals 2 and 3, and (c) Interval 4. The susceptibilities are normalized to the room temperature values.

Day diagram [Day *et al.*, 1977] to estimate the magnetic domain states of magnetic particles for these two intervals (Figure 10b). As expected, all of the data fall into the pseudo-single domain (PSD) field for (titano)magnetite, however, samples from Interval 4 overwhelmingly plot nearer the single domain (SD) field than samples from Interval 1. This suggests that there is a fine-grained magnetic enhancement in the mud between 3.24 and 14 m.

5. Discussion

[32] Previous studies have generally shown that magnetic mineral diagenesis begins with iron oxide reduction, which leads to dissolution of the finest-grained iron oxides (largely ferrimagnetic grains such as magnetite), followed by the destruction of the remaining coarse grains [e.g., Karlin and Levi, 1983; Bloemendal *et al.*, 1993]. In this diagenetic stage, ferric (Fe^{3+}) ions dissociated from iron oxides become reduced into the divalent state. Later, during sulfate reduction, dissolved ferrous (Fe^{2+}) ions react with H_2S , whose most important source is the reduction of interstitial dissolved sulfate by bacteria that use organic matter as a reducing agent, to form a succession of iron sulfide phases in the following order: mackinawite (with a composition similar to $\text{FeS}_{0.9}$), greigite (Fe_3S_4), and finally pyrite (FeS_2) [Berner, 1984].

[33] The studied sediments from the Korea Strait are lithologically homogeneous, therefore the systematic down-core magnetic changes observed in the mud sections of the SSDP-102 and SSDP-103 cores must be due to post-depositional diagenetic processes. In particular, the magnetic changes are not accompanied by any significant geochemical changes. The only significant change recorded in the measured chemical parameters is the change in total Fe content at ~ 3 m in the SSDP-102 core (Figure 4), which is not reflected in the magnetic profiles for this core (Figure 6). Lack of pore water chemistry data makes it impossible to determine whether this chemical change relates to an active redox front. It is unlikely that this change is related to a shift

in provenance of detrital minerals since the other chemical parameters are nearly constant through most of the core. No such similar shift is observed in the SSDP1-3 core. Nevertheless, the homogeneous nature of the sediment and the almost constant geochemical properties indicate that the rapid down-core decrease in concentration of magnetic grains, as observed in the two studied cores, which has been widely recognized in deep-water marine sediments [e.g., Karlin, 1990a; Leslie *et al.*, 1990], is also a characteristic magnetic signature of early diagenesis in these continental shelf sediments.

5.1. Diagenetic Stages for Magnetic Minerals in Continental Shelf Sediments

[34] Post-middle-Holocene mud from the Korea Strait has recorded a more detailed picture of magnetic mineral diagenesis than has been reported in deeper water settings because of the extremely high sedimentation rates in this continental shelf setting. Interval 1 in both cores is marked by the highest values of all concentration-dependent bulk magnetic parameters (NRM, χ , ARM, SIRM and HIRM), the highest S_{300} values and the lowest total sulfur content in the entire studied mud section. This interval is therefore interpreted to be the least affected by early diagenetic influences. The main magnetic minerals in this part of the cores (magnetite and hematite) can be regarded as the primary detrital magnetic minerals in the underlying mud prior to diagenetic modification.

[35] Ubiquitous pyrite formation in the mud below Interval 1 in both cores indicates that, as has been widely reported in deep-water marine sediments [e.g., Canfield and Berner, 1987], early diagenesis has proceeded through the early stages of reduction dissolution of detrital ferrimagnetic and possibly high coercivity iron oxides to the later stage of sulfate reduction. Magnetic measurements have unambiguously revealed the characteristic magnetic mineralogical variations in these rapidly accumulated sediments. We can identify 3 obvious diagenetic stages that influence the magnetic properties in these continental shelf

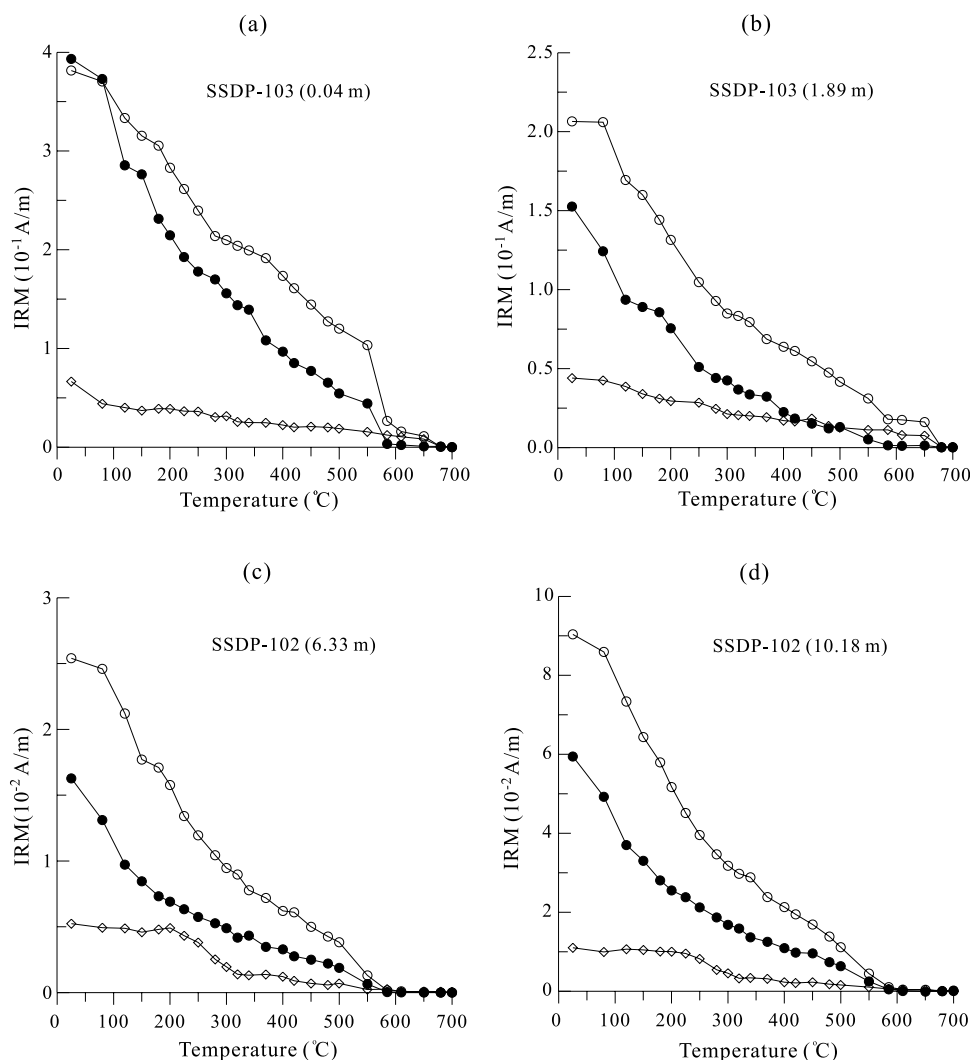


Figure 9. Representative thermal demagnetization data for a 3-axis IRM for: (a) Interval 1, (b) Intervals 2 and 3, and (c, d) Interval 4 for the SSDP-102 and SSDP-103 cores. Open diamonds represent the high coercivity (0.5–2.7 T) component; open circles represent the intermediate coercivity (0.05–0.5 T) component; and solid circles represent the low coercivity (<0.05 T) component.

sediments (initial, middle and late stages), which correspond to Intervals 2, 3 and 4, respectively.

[36] The initial diagenetic stage, observed in Interval 2, begins with a sharp decrease in ferrimagnetic mineral concentrations. These concentrations decline progressively with depth until the absolute minimum abundance is reached at the end of this stage, as suggested by changes in S_{300} values. This stage is associated with an average 30% (core SSDP-103; Figure 7) to 55% (core SSDP-102) depletion of the high coercivity component (i.e., hematite), as shown by variations of HIRM values in both cores. Hematite is much less severely depleted than magnetite, which therefore makes hematite relatively more important as the magnetite component is progressively dissolved.

[37] The middle diagenetic stage, observed in Interval 3, is marked by the further depletion of high coercivity grains (hematite) with depth (and time). At the base of Interval 3, this hematite depletion terminates with 82% (core SSDP-102) to 88% (core SSDP-103) of the primary

hematite component having disappeared, as reflected by changes in the HIRM values in the two cores. The depletion of hematite with depth is coupled with down-core decreases of χ , SIRM and ARM and a down-core increase of S_{300} values down to the base of Interval 3. These observations suggest that the bulk magnetic mineral concentration is reduced to almost minimum values at the end of this diagenetic stage. The relatively minor decrease in NRM intensity in this interval probably indicates that the decline in hematite concentration had little effect on the NRM.

[38] The late diagenetic stage, as observed in Interval 4, is characterized by authigenic production of fine-grained ferrimagnetic minerals. The reductive dissolution of ferrimagnetic minerals during early diagenesis is a grain size-selective process, which leads to initial dissolution of the finest-grained iron oxides, followed by the destruction of the remaining coarse grains [Karlin and Levi, 1983]. Interval 4, which has been subjected to the initial and middle diagenetic stages like the overlying intervals,

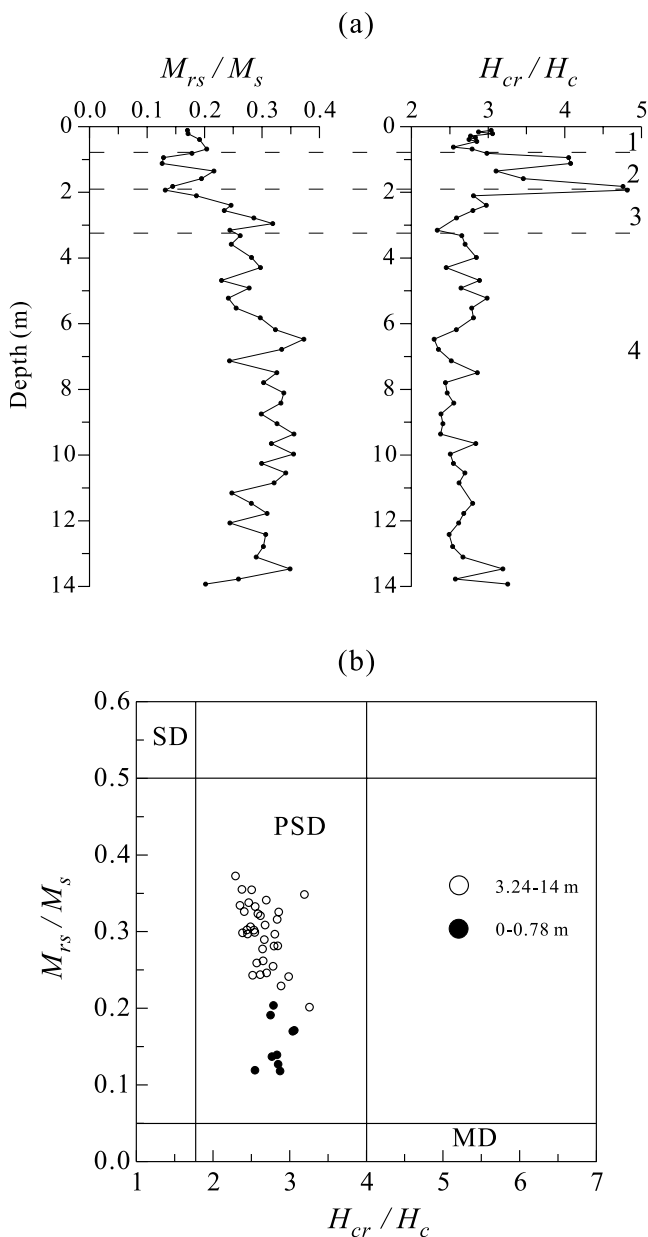


Figure 10. (a) Down-core variations of M_{rs}/M_s and H_{cr}/H_c in the mud section of the SSDP-102 core. (b) Plot of M_{rs}/M_s vs. H_{cr}/H_c (after Day *et al.* [1977]) for samples from Interval 1 (0 to 0.78 m) and Interval 4 (3.24 to 14 m).

would only have retained, if any, the largest magnetic grains. On the contrary, however, the ferrimagnetic minerals in Interval 4 are even finer than in Interval 1 (Figure 10), which is the least affected by diagenetic alteration. Where have these finer ferrimagnetic grains come from if most, if not all, of the fine-grained detrital magnetic minerals were reductively dissolved predominantly in the initial diagenetic stage, as is the case in Interval 2? The fine-grained magnetic enhancement can be reasonably interpreted to be of authigenic origin. Thermomagnetic measurements (Figure 9) suggest that greigite is present in the sediments of Interval 4. Sedimentary greigite has been consistently found to have

SD-like magnetic properties [Snowball, 1991; Roberts, 1995], which is consistent with the observed finer ferrimagnetic grain sizes observed for Interval 4 (Figure 10). Admixture of newly formed authigenic SD greigite with coarse-grained (MD) magnetite, which is the only magnetite that is likely to have survived diagenetic dissolution, would give rise to lower M_{rs}/M_s and higher H_{cr}/H_c values (averaging to PSD-like values) than would be expected for sedimentary greigite (Figure 10) [Roberts, 1995]. The most likely mechanism for formation and preservation of greigite in these sediments is arrest of the pyritization process [e.g., Berner, 1984]. Downward consumption of pore water sulfate, as a result of the lengthened diffusion pathway for sulfate from the overlying seawater reservoir, is unlikely to contribute to arrested pyritization even in such high sedimentation rate environments. The higher C_{org} contents in Interval 4 could have contributed to greigite preservation through a mechanism suggested by Kao *et al.* [2004]. Fine-grained greigite-bearing sediments from southwestern Taiwan have higher C_{org} contents and high iron activity compared to sediments not containing greigite. Kao *et al.* [2004] argue that high iron activity might have suppressed sulfate reduction and removed reduced sulfur so effectively that pyritization was arrested or retarded, which would have favored preservation of intermediate greigite.

5.2. Diagenetic Effects on Magnetic Records

[39] Early diagenesis has greatly modified the magnetic assemblages of the studied post-middle-Holocene mud section in the SSDP-102 and SSDP-103 cores, which has resulted in substantial loss of the detrital magnetic minerals. In the initial and middle stages of magnetic mineral diagenesis, as in Intervals 2 and 3 from both studied cores, the net result of diagenesis is a progressive chemical “cleaning”, with removal of most of the detrital magnetic minerals. These diagenetic processes have also produced a small, but noticeable, magnetic enhancement due to authigenic production of greigite in the deepest observed diagenetic stage (Interval 4). The greigite that has formed in these sediments has clearly grown authigenically at depths in excess of 3 m below the sediment-water interface. While it is known that remagnetizations, often with contradictory polarities, can occur as a result of authigenic formation of greigite or pyrrhotite [e.g., Florindo and Sagnotti, 1995; Horng *et al.*, 1998; Dinarès-Turell and Dekkers, 1999; Jiang *et al.*, 2001; Weaver *et al.*, 2002], detailed constraints on the timing of remanence acquisition for greigite in active depositional environments are sparse. Roberts and Turner [1993] and others have warned of the possibility of substantial delayed remanence acquisition in greigite-bearing sediments; however, this is the first clear demonstration from an active depositional environment for a delay of thousands of years for acquisition of a magnetization carried by greigite. This detailed view of diagenetic processes in continental shelf sediments suggests that studies of geomagnetic field behavior from such sediments should be conducted with care. Paleoclimatographic and paleoclimatic studies based on the magnetic properties of shelf sediments with high sedimentation rates like those in the Korea Strait are also unlikely to provide a

meaningful signature associated with syn-depositional environmental processes.

6. Conclusions

[40] Our results suggest that the studied mud section in post-middle-Holocene continental shelf sediments from the Korea Strait is rather uniform lithologically and geochemically and that the magnetic mineral assemblages have undergone profound post-depositional diagenetic alteration. The strata in the studied cores can be obviously divided into the following four intervals, in descending order, which define different diagenetic stages in which marked changes in magnetic mineralogy are observed. Interval 1 is the least affected by diagenesis and has the highest magnetic mineral concentrations and the lowest total sulfur contents in the studied mud section. The main magnetic components include magnetite and hematite, with magnetite being dominant. Interval 2, which represents the initial diagenetic stage, is marked by a sharp decrease in the concentration of magnetite, followed by a gradual decline until a minimum is reached at the base of this interval. Hematite was depleted by 30% to 55% in this interval, which also has far higher total sulfur content than the overlying interval, which is consistent with the observed formation of pyrite. Interval 3, in which the middle diagenetic stage is observed, is characterized by a progressive loss of hematite down-core. At the base of this interval, 82% to 88% of the hematite component was depleted and the bulk magnetic mineral concentration was reduced to the lowest value in the entire studied mud section. Interval 4, which records the latest diagenetic stage, has an increasing fine-grained ferrimagnetic enhancement with depth. The newly formed authigenic fine-grained magnetic mineral is greigite.

[41] Diagenetic modification of the magnetic mineralogy of continental shelf sediments will have severely adverse effects on paleoceanographic and paleoclimatic studies that use magnetic properties as indicators of paleoceanographic and paleoclimatic change. Additionally, demonstration that greigite can authigenically grow at depths in excess of 3 m below the sediment-water interface will have adverse implications for detailed studies of geomagnetic field behavior from continental shelf sediments in cases where greigite contributes substantially to the magnetization.

[42] **Acknowledgments.** This work was supported by the National Natural Science Foundation of China through grant #49976012. APR acknowledges support from the Royal Society of London and from the Leverhulme Trust. We thank Mike Jackson, Paul Kelso and Graham Borradaile (Associate Editor) for their reviews, which helped to improve the paper.

References

- Berner, R. A. (1984), Sedimentary pyrite formation: An update, *Geochim. Cosmochim. Acta*, *48*, 605–615.
- Bloemendal, J., J. W. King, A. Hunt, P. B. DeMenocal, and A. Hayashida (1993), Origin of the sedimentary magnetic record at Ocean Drilling Program sites on the Owen Ridge, western Arabian Sea, *J. Geophys. Res.*, *98*, 4199–4219.
- Cannfield, D. E., and R. A. Berner (1987), Dissolution and pyritization of magnetite in anoxic marine sediments, *Geochim. Cosmochim. Acta*, *51*, 645–660.
- Day, R., M. Fuller, and V. A. Schmidt (1977), Hysteresis properties of titanomagnetites: Grain size and compositional dependence, *Phys. Earth Planet. Inter.*, *13*, 260–267.
- Dekkers, M. J. (1989), Magnetic properties of natural pyrrhotite. II. High- and low-temperature behaviour of *J_rs* and TRM as function of grain size, *Phys. Earth Planet. Inter.*, *57*, 266–283.
- Dekkers, M. J., C. G. Langereis, S. P. Vriend, P. J. M. van Santvoort, and G. J. de Lange (1994), Fuzzy c-means cluster analysis of early diagenetic effects on natural remanent magnetisation acquisition in a 1.1 Myr piston core from the Central Mediterranean, *Phys. Earth Planet. Inter.*, *85*, 155–171.
- Dekkers, M. J., H. F. Passier, and M. A. A. Schoonen (2000), Magnetic properties of hydrothermally synthesized greigite (Fe₃S₄)—II. High- and low-temperature characteristics, *Geophys. J. Int.*, *141*, 809–819.
- Dinarès-Turell, J., and M. J. Dekkers (1999), Diagenesis and remanence acquisition in the Lower Pliocene Trubi marls at Punta di Maiata (southern Sicily): Palaeomagnetic and rock magnetic observations, *Geol. Soc. London Spec. Publ.*, *151*, 53–69.
- Florindo, F., and L. Sagnotti (1995), Palaeomagnetism and rock magnetism at the upper Pliocene Valle Ricca (Rome, Italy) section, *Geophys. J. Int.*, *123*, 340–354.
- Folk, R. L., and W. C. Ward (1957), Brazos River bar: A study in the significance of grain size parameters, *J. Sediment. Petrol.*, *31*, 514–519.
- Geiss, C. E., and S. K. Banerjee (1997), A multi-parameter rock magnetic record of the last glacial-interglacial paleoclimate from south-central Illinois, USA, *Earth Planet. Sci. Lett.*, *152*, 203–216.
- Hong, C.-S., M. Torii, K. S. Shea, and S.-J. Kao (1998), Inconsistent magnetic polarities between greigite- and pyrrhotite/magnetite-bearing marine sediments from the Tsailiao-chi section, southwestern Taiwan, *Earth Planet. Sci. Lett.*, *164*, 467–481.
- Jiang, W.-T., C.-S. Hong, A. P. Roberts, and D. R. Peacor (2001), Contradictory magnetic polarities in sediments and variable timing of neof ormation of authigenic greigite, *Earth Planet. Sci. Lett.*, *193*, 1–12.
- Jin, J. H., and S. K. Chough (1998), Partitioning of transgressive deposits in the southeastern Yellow Sea: A sequence stratigraphic interpretation, *Mar. Geol.*, *149*, 79–92.
- Kao, S.-J., C.-S. Hong, A. P. Roberts, and K.-K. Liu (2004), Carbon-sulfur-iron relationships in sedimentary rocks from southwestern Taiwan: Influence of geochemical environment on greigite and pyrrhotite formation, *Chem. Geol.*, *203*, 153–168.
- Karlin, R. (1990a), Magnetite diagenesis in marine sediments from the Oregon continental margin, *J. Geophys. Res.*, *95*, 4405–4419.
- Karlin, R. (1990b), Magnetic mineral diagenesis in suboxic sediments at Bettis Site W-N, NE Pacific Ocean, *J. Geophys. Res.*, *95*, 4421–4436.
- Karlin, R., and S. Levi (1983), Diagenesis of magnetic minerals in recent haemipelagic sediments, *Nature*, *303*, 327–330.
- Karlin, R., and S. Levi (1985), Geochemical and sedimentological control of the magnetic properties of hemipelagic sediments, *J. Geophys. Res.*, *90*, 10,373–10,392.
- Karlin, R., M. Lyle, and G. R. Heath (1987), Authigenic magnetite formation in suboxic marine sediments, *Nature*, *326*, 490–493.
- Kim, M. S., K. S. Chu, and O. S. Kim (1986), Investigation of some influence of the Nakdong River water on marine environment in the estuarine area using Landsat imagery, *Rep. Korea Ministry Sci. Tech.*, *93*–147, Korea. Minist. of Sci. and Technol., Gwacheon City, Korea.
- King, J., and J. E. T. Channell (1991), Sedimentary magnetism, environmental magnetism, and magnetostratigraphy, *Rev. Geophys.*, *29*, 358–370, suppl.
- Korean Institute of Geology, Mining and Materials (2000), Study on Quaternary stratigraphy and environmental changes in the Korea South Sea, *Tech. Rep.*, 677 pp., Taejon, Korea.
- Krs, M., M. Krsová, L. Koulíková, P. Pruner, and F. Valín (1992), On the applicability of oil shale to paleomagnetic investigations, *Phys. Earth Planet. Inter.*, *70*, 178–186.
- Larrasoana, J. C., A. P. Roberts, J. S. Stoner, C. Richter, and R. Wehausen (2003), A new proxy for bottom-water ventilation based on diagenetically controlled magnetic properties of eastern Mediterranean sapropel-bearing sediments, *Palaeogeogr., Palaeoclimatol., Palaeoecol.*, *190*, 221–242.
- Leslie, B. W., S. P. Lund, and D. E. Hammond (1990), Rock magnetic evidence for the dissolution and authigenic growth of magnetic minerals within anoxic marine sediments of the California continental borderland, *J. Geophys. Res.*, *95*, 4437–4452.
- Liu, J. P., J. D. Milliman, and S. Gao (2002), The Shandong mud wedge and post-glacial sediment accumulation in the Yellow Sea, *Geo Mar. Lett.*, *21*, 212–218.
- Lowrie, W. (1990), Identification of ferromagnetic minerals in a rock by coercivity and unblocking temperature properties, *Geophys. Res. Lett.*, *17*, 159–162.
- Nam, S. I., J. H. Chang, S. P. Kim, G. S. Kong, D. G. Yoo, and A. Mackensen (2003), Paleoenvironmental changes in the Korea Strait

- during the post-glacial marine transgression, *XVI INQUA Congress Programs with Abstracts*, 214 pp., Desert Res. Inst., Reno, Nevada.
- Park, S. C., and S. D. Lee (1994), Depositional patterns of sand ridges in tide-dominated shallow water environments: Yellow Sea coast and South Sea of Korea, *Mar. Geol.*, **120**, 89–103.
- Park, S. C., and D. G. Yoo (1988), Depositional history of Quaternary sediments on the continental shelf off the southeastern coast of Korea (Korea Strait), *Mar. Geol.*, **79**, 65–75.
- Park, S. C., and D. G. Yoo (1992), Deposition of coarse-grained sediments in the Korea Strait during late Pleistocene low sea level, *Geo. Mar. Lett.*, **12**, 19–23.
- Park, S. C., K. M. Jang, and S. D. Lee (1990), High-resolution seismic study of modern fine-grained deposits: Inner shelf off the southeastern coast of Korea, *Geo. Mar. Lett.*, **10**, 45–149.
- Park, S. C., K. W. Lee, and Y. I. Song (1995), Acoustic characters and distribution pattern of modern fine-grained deposits in a tide-dominated coastal bay: Jinhae Bay, southeast Korea, *Geo. Mar. Lett.*, **15**, 77–84.
- Park, S. C., S. K. Hong, and D. C. Kim (1996), Evolution of late Quaternary deposits on the inner shelf of the South Sea of Korea, *Mar. Geol.*, **131**, 219–232.
- Park, S. C., D. G. Yoo, K. W. Lee, and H. H. Lee (1999), Accumulation of recent muds associated with coastal circulations, southeastern Korea Sea (Korea Strait), *Cont. Shelf Res.*, **19**, 589–608.
- Park, S. C., D. G. Yoo, C. W. Lee, and E. I. Lee (2000), Last glacial sea-level changes and paleogeography of the Korea (Tsushima) Strait, *Geo. Mar. Lett.*, **20**, 64–71.
- Park, S. C., H. S. Han, and D. G. Yoo (2003), Transgressive sand ridges on the mid-shelf of the southern sea of Korea (Korea Strait): Formation and development in high-energy environments, *Mar. Geol.*, **193**, 1–18.
- Reynolds, R. L., M. L. Tuttle, C. A. Rice, N. S. Fishman, J. A. Karachewski, and D. M. Sherman (1994), Magnetization and geochemistry of greigite-bearing Cretaceous strata, North Slope basin, Alaska, *Am. J. Sci.*, **294**, 485–528.
- Ro, Y. J., M. J. Park, S. R. Lee, and J. C. Lee (1995), Structures and variability of the T-S field and the current across the Korea Strait, *J. Oceanol. Soc. Korea*, **30**, 237–249.
- Roberts, A. P. (1995), Magnetic properties of sedimentary greigite (Fe₃S₄), *Earth Planet. Sci. Lett.*, **134**, 227–236.
- Roberts, A. P., and B. J. Pillans (1993), Rock magnetism of Lower/Middle Pleistocene marine sediments, Wanganui Basin, New Zealand, *Geophys. Res. Lett.*, **20**, 839–842.
- Roberts, A. P., and G. M. Turner (1993), Diagenetic formation of ferrimagnetic iron sulphide minerals in rapidly deposited marine sediments, South Island, New Zealand, *Earth Planet. Sci. Lett.*, **115**, 257–273.
- Roberts, A. P., J. S. Stoner, and C. Richter (1999), Diagenetic magnetic enhancement of sapropels from the eastern Mediterranean Sea, *Mar. Geol.*, **153**, 103–116.
- Robinson, S. G. (1986), The late Pleistocene palaeoclimatic record of North Atlantic deep-sea sediments revealed by mineral-magnetic measurements, *Phys. Earth Planet. Inter.*, **42**, 22–47.
- Robinson, S. G., J. T. S. Sahota, and F. Oldfield (2000), Early diagenesis in North Atlantic abyssal plain sediments characterized by rock-magnetic and geochemical indices, *Mar. Geol.*, **163**, 77–107.
- Sakaguchi, T., J. G. Burgess, and T. Matsunaga (1993), Magnetite formation by a sulphate-reducing bacterium, *Nature*, **365**, 47–49.
- Saito, Y. (1993), Fundamental study of sequence stratigraphy of the latest Pleistocene-Holocene sequence on the Pacific side of Northeast Japan, Ph.D. thesis, Kyushu Univ., 106 pp.
- Snowball, I. F. (1991), Magnetic hysteresis properties of greigite (Fe₃S₄) and a new occurrence in Holocene sediments from Swedish Lapland, *Phys. Earth Planet. Inter.*, **68**, 32–40.
- Snowball, I., and R. Thompson (1990), A stable chemical remanence in Holocene sediments, *J. Geophys. Res.*, **95**, 4471–4479.
- Stockhausen, H., and N. Thouveny (1999), Rock-magnetic properties of Eemian maar lake sediments from Massif Central, France: A climatic signature?, *Earth Planet. Sci. Lett.*, **173**, 299–313.
- Stolz, J. F., S. B. R. Chang, and J. L. Kirschvink (1986), Magnetotactic bacteria and single-domain magnetite in hemipelagic sediments, *Nature*, **321**, 849–851.
- Tarduno, J. A. (1994), Temporal trends of magnetic dissolution in the pelagic realm: Gauging paleoproductivity?, *Earth Planet. Sci. Lett.*, **123**, 39–48.
- Thompson, R., and F. Oldfield (1986), *Environmental Magnetism*, Allen and Unwin, London, 229 pp.
- Torii, M., K. Fukuma, C.-S. Horng, and T.-Q. Lee (1996), Magnetic discrimination of pyrrhotite- and greigite-bearing sediment samples, *Geophys. Res. Lett.*, **23**, 1813–1816.
- Verosub, K. L., and A. P. Roberts (1995), Environmental magnetism: Past, present, and future, *J. Geophys. Res.*, **100**, 2175–2192.
- Vigliotti, L. (1997), Magnetic properties of light and dark sediment layers from the Japan Sea: Diagenetic and paleoclimatic implications, *Quat. Sci. Rev.*, **16**, 1093–1114.
- Weaver, R., A. P. Roberts, and A. J. Barker (2002), A late diagenetic (synfolding) magnetization carried by pyrrhotite: Implications for paleomagnetic studies from magnetic iron sulphide-bearing sediments, *Earth Planet. Sci. Lett.*, **200**, 371–386.
- Yoo, D. G., and S. C. Park (1997), Late Quaternary lowstand wedges on the shelf margin and trough region of the Korea Strait, *Sediment. Geol.*, **109**, 121–133.
- Yoo, D. G., and S. C. Park (2000), High-resolution seismic study as a tool for sequence stratigraphic evidence of high-frequency sea-level changes: Latest Pleistocene-Holocene example from the Korea Strait, *J. Sediment. Res.*, **70**, 296–309.
- Yoo, D. G., S. C. Park, W. C. Shin, and W. S. Kim (1996), Near-surface seismic facies at the Korea Strait shelf margin and trough region, *Geo. Mar. Lett.*, **16**, 49–56.
- Yoo, D. G., J. H. Chang, S. I. Nam, S. P. Kim, and S. C. Park (2003), Evolution of late Quaternary deposits on the inner shelf off the southeastern coast of Korea (Korea Strait), *XVI INQUA Congress Programs with Abstracts*, 214 pp., Desert Res. Inst., Reno, Nevada.
- Zhao, X. (1984), Studies of the evolution of China's coast (in Chinese), pp. 178–186, Sci. and Technol. Press of Fujian.

J.-H. Chang, Korean Institute of Geology, Mining and Material, Taejon, 305-350, Korea.

S. Li and J. Liu, Qingdao Institute of Marine Geology, China Geological Survey, Qingdao 266071, China. (liujian0550@vip.sina.com)

A. P. Roberts, School of Ocean and Earth Science, University of Southampton, Southampton Oceanography Centre, Southampton SO14 3ZH, UK.

R. Zhu, Institute of Geology and Geophysics, Chinese Academy of Sciences, Beijing 100029, China.